GSA DATA REPOSITORY 2014338

East African lake evidence for Pliocene millennial-scale climate variability

K.E. Wilson, M.A. Maslin, M.J. Leng, J.D. Kingston, A.L. Deino, R.K. Edgar, A.W. Mackay

1). Chronology (from Deino et al., 2006)

- $^{40}Ar/^{39}Ar$ ages of 3 tuff layers (above, below and within unit #4) and position of palaeomagnetic Gauss/Matuyama (G/M) reversal boundary constrain chronology of unit #4.
- Ages adjusted to Astronomical Polarity Time Scale (APTS) on basis of independent calibration to G/M boundary at 2.610 Ma.
- Sedimentation rates for Rift Valley diatomites range from 10-100 cm/kyr (Gasse, 1980; Deino and Potts, 1990).
- Linear sedimentation rate (72 cm/kyr) is assumed as initial basis for age model.
- Non-uniform sedimentation rates, based on natural transgressive/regressive lake cycles are also considered:
    - Based on presence of non-laminated diatomaceous clay (upper 150cm, regressive phase), we assign an accumulation rate of 100 cm/kyr.
    - Estimated sedimentation rate for the lowest 10 cm (transgressive phase) of the unit = 10 cm/kyr. Ages are interpolated accordingly.

2). Geochemistry and Mass-balance Correction (described in full in Wilson et al., 2014)

- Cleaning methodology outlined in Wilson et al. (2014).
- $\delta^{18}O_{diatom}$ data precision can be compromised by the presence of tephras, clays and carbonates, which remain within purified samples (Morley et al., 2004; Brewer et al., 2008).
- XRF data analysed using Principal Components Analysis to identify different contaminants (tephra and clay).
- $\delta^{18}O_{diatom}$ data were corrected ($\delta^{18}O_{modelled}$) for the effects of contamination using a three end-member mass-balance model:

$$\delta^{18}\mathrm{O}_{\mathrm{modelled}} = \delta^{18}O_{sample} - \frac{\left[\left(\frac{\%tephra}{100}\ x\ \delta^{18}O_{tephra}\right) + \left(\frac{\%clay}{100}\ x\ \delta^{18}O_{clay}\right)\right]}{\frac{\%diatom}{100}}$$

3). Ti/Al Data

- Ti/Al data (Fig. 2) from Ocean Drilling Program (ODP) Site 721/722 in the Arabian Sea (Wilson, 2011) illustrates extra-regional evidence for changes in the strength of Indian Ocean monsoonal circulation.
- Elemental analysis of ODP 721 (16°40.636 'N, 59°51.879 'E; water depth 1,945 m) and 722 (16°37.312 'N, 59°47.755 'E; water depth 2,028 m) sediments was conducted using an Avaatech XRF core scanner at UCL.

- Core sections were scanned three times at 2 mm intervals and raw count data calibrated using WinAxil and WinBatch conversion software.
- Chronology for ODP 721/722 (Wilson, 2011) is based on a revision of pre-existing age-models (Murray and Prell, 1991; Clemens et al., 1996) using detailed benthic oxygen isotope stratigraphy tied to palaeomagnetic reversal data and the LR04 benthic isotope stack (Lisiecki and Raymo, 2005).
- Ti/Al data was interpolated onto the same sampling grid as the lower resolution $\delta^{18}O_{modelled}$ record with a cubic-spline interpolation technique using MATLAB v. R2013a.

4). Spectral Analysis

- Spectral analysis of $\delta^{18}O_{modelled}$ data (using linear timescale) conducted using the Lomb-Scargle Fourier Transform method (Trauth, 2010).
- Power spectrum (Fig. S1) reveals dominant spectral peaks which correspond to periodicities of ~9 kyr (f = 0.111), ~1.65 kyr (f = 0.604), ~965 yr (f = 1.036) and ~583 yr (f = 1.714).
- Due to the timespan and resolution (n=42) of the record, minimal importance is assigned to cycles of ~9 kyr and 583 yr which reflect periodicities both too long and too short to be representative of variation within the data.

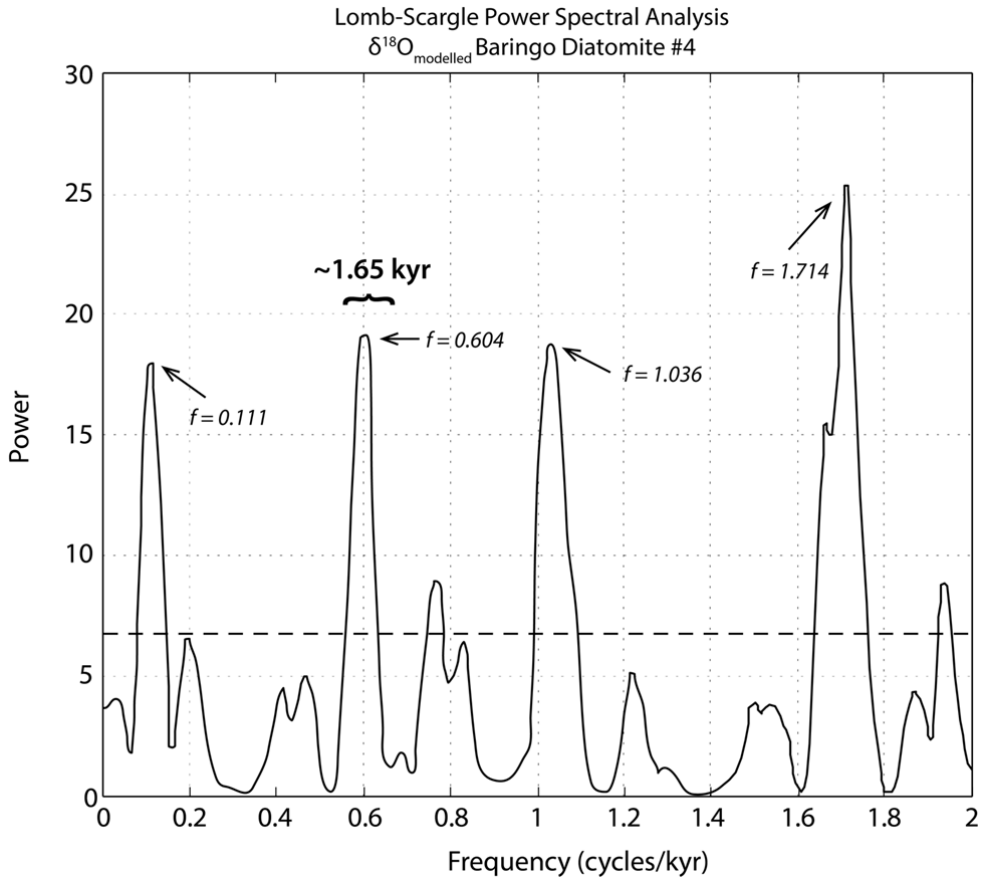

Figure DR1. Power spectral plot for $\delta^{18}O_{modelled}$ values from Baringo diatomite unit #4 showing dominant periodicities at frequencies of 0.111 (~9 kyr), 0.604 (~1.65 kyr), 1.036 (965 yr) and 1.714 (583 yr). Dashed line indicates 95% significance level.

References

Brewer, T.S., Leng, M.J., Mackay. A.W., Lamb, A.L., Tyler, J.J., and Marsh, N.G., 2008, Unravelling contamination signals in biogenic silica oxygen isotope composition: The role of major and trace element geochemistry: Journal of Quaternary Science, v. 23, p. 321-330.

Clemens, S.C., Murray, D.W., and Prell, W.L., 1996, Nonstationary phase of the Plio-Pleistocene, Asian monsoon: Science, v. 274, p. 943-948.

Deino, A.L., Potts, R., 1990, Single-crystal 40Ar/39Ar dating of the Olorgesailie Formation, southern Kenya Rift. Journal of Geophysical Research B., Solid Earth Planets, v. 95, p. 8453-8470.

Deino, A.L., Kingston, J.D., Glen, J.M., Edgar, R.K., and Hill, A., 2006, Precessional forcing of lacustrine sedimentation in the late Cenozoic Chemeron Basin, Central Kenya Rift, and the calibration of the Gauss/Matuyama boundary: Earth and Planetary Science Letters, v. 247, p. 41-60.

Gasse, F., 1980, Les diatomées lacustres plio-pléistocénes du Gadeb (Éthiopie): systématique, paléoécologie, biostratigraphie: Revue Algolgique, Mémoire hors-série no. 3, 62 pl., 249 p.

Lisiecki, L.E., and Raymo, M.E., 2005, A Pliocene-Pleistocene stack of 57 globally distributed benthic δ18O records: Paleoceanography, v. 20, PA1003, doi:10.1029/2004PA001071.

Morley, D.W., Leng, M.J., Mackay, A.W., Sloane, H.J., Rioual, P., and Battarbee, R.W., 2004, Cleaning of lake sediment samples for diatom oxygen isotope analysis: Journal of Palaeolimnology, v. 31, p. 391–401.

Murray, D.W., and Prell, W.L., 1991, Pliocene to Pleistocene variations in calcium carbonate,

organic carbon and opal on the Owen Ridge, Northern Arabian Sea: Proceedings of the Ocean Drilling Program, Scientific Results, v. 117, p. 343-363.

Trauth, M.H., 2010, MATLAB® Recipes for Earth Sciences, Third Edition. Springer-Verlag, Berlin. 336pp.

Wilson, K.E., 2011, Plio-Pleistocene reconstruction of East African and Arabian Sea palaeoclimate. Ph.D. thesis, UCL, London: 301 pp.

Wilson, K.E., Leng, M.J., Mackay, A.W., 2014, The use of multivariate statistics to resolve multiple contamination signals in the oxygen isotope analysis of biogenic silica: Journal of Quaternary Science, in press, doi: 10.1002/jqs.2729.

Table DR1. Data from analysis of Baringo Diatomite unit #4

Sample No.	Section Height (cm)	Linear Age (Ma)	Non-uniform Age (Ma)	Proportion *Stephanodiscus*	Calculated Contamination (%)			$\delta^{18}O$ (per mil V-SMOW)		
					Tephra	Clay	Total	$\delta^{18}O_{diatom}$	$\delta^{18}O_{modelled}$	±
4054	10	2.616863	2.616000	0.010						
4055	20	2.616725	2.615865	0.059	3.01	5.67	8.68	31.83	33.64	0.90
4056	30	2.616588	2.615730	0.010						
4057	40	2.616450	2.615595	0.005	2.50	5.20	7.70			
4058	50	2.616313	2.615460	0.063	2.79	2.51	5.30	33.61	34.82	0.60
4059	60	2.616175	2.615325	0.067	4.18	3.11	7.28	34.32	36.08	0.88
4060	70	2.616038	2.615190	0.095	0.44	0.84	1.28	34.20	34.47	0.14
4061	80	2.615900	2.615056	0.049	0.91	5.02	5.93	34.17	35.46	0.64
4062	90	2.615763	2.614921	0.042	0.66	1.13	1.79	35.75	36.16	0.21
4063	100	2.615625	2.614786	0.454	3.20	2.54	5.73	34.84	36.23	0.70
4064	110	2.615488	2.614651	0.016	6.39	3.10	9.49	34.37	36.77	1.20
4065	120	2.615350	2.614516	0.082	1.02	6.17	7.19	33.99	35.56	0.78
4066	130	2.615213	2.614381	0.177	2.63	6.86	9.49	32.44	34.46	1.01
4067	140	2.615075	2.614246	0.178	5.28	8.45	13.73	33.08	36.33	1.62
4069	160	2.614800	2.614111	0.056	23.42	23.00	46.42	22.34	31.16	4.41
4070	170	2.614663	2.613976	0.162	3.69	5.92	9.61	32.72	34.85	1.06
4071	180	2.614525	2.613841	0.286	3.11	16.44	19.54	32.63	37.23	2.30
4072	190	2.614388	2.613706	0.388						
4073	200	2.614250	2.613571	0.354	3.58	14.62	18.20			
4074	210	2.614113	2.613437	0.554				35.99		
4075	220	2.613975	2.613302	0.702	1.37	7.02	8.39			
4076	230	2.613838	2.613167	0.586	2.66	2.52	5.18	36.22	37.54	0.66
4077	240	2.613700	2.613032	0.446	1.19	10.03	11.22			
4078	250	2.613563	2.612897	0.621	1.23	0.01	1.24	35.92	36.25	0.16
4079	260	2.613425	2.612762	0.688	3.00	9.06	12.06	33.48	36.25	1.38
4080	270	2.613288	2.612627	0.549	2.33	0.48	2.81	34.76	35.46	0.35
4081	280	2.613150	2.612492	0.387	2.06	7.99	10.05			
4082	290	2.613013	2.612357	0.325	1.78	1.55	3.33	34.20	34.96	0.38
4083	300	2.612875	2.612222	0.213	2.49	15.40	17.90	31.98	35.95	1.98
4084	310	2.612738	2.612087	0.315	2.71	5.07	7.78	35.27	37.16	0.95
4085	320	2.612600	2.611952	0.306	2.13	18.42	20.56			
4086	330	2.612463	2.611817	0.140						
4087	340	2.612325	2.611683	0.219	3.01	11.20	14.21	32.25	35.36	1.56
4088	350	2.612188	2.611548	0.410	1.61	2.84	4.46	34.50	35.51	0.51
4089	360	2.612050	2.611413	0.248	1.67	11.28	12.95			
4090	370	2.611913	2.611278	0.414	0.89	1.92	2.81	35.26	35.91	0.32
4091	380	2.611775	2.611143	0.136	5.12	10.64	15.77	33.44	37.27	1.92
4092	390	2.611638	2.611008	0.689	1.66	1.23	2.89	35.87	36.58	0.36
4093	400	2.611500	2.610873	0.187	1.56	9.28	10.85			
4094	410	2.611363	2.610738	0.178	3.13	0.82	3.95	35.37	36.37	0.50
4095	420	2.611225	2.610603	0.148	2.06	5.67	7.73	32.03	33.61	0.79
4096	430	2.611088	2.610468	0.253	0.00	0.00	0.00	35.47	35.44	0.01
4097	440	2.610950	2.610333	0.407	0.96	5.48	6.44			
4098	450	2.610813	2.610198	0.300	1.88	0.11	1.77	35.94	36.42	0.24
4099	460	2.610675	2.610063	0.518				32.32		
4100	470	2.610538	2.609929	0.404	6.02	1.03	7.06	35.18	37.04	0.93
4101	480	2.610400	2.609794	0.358	2.69	9.18	11.87			

Table DR1 continued.

Sample No.	Section Height (cm)	Linear Age (Ma)	Non-uniform Age (Ma)	Proportion *Stephanodiscus*	Calculated Contamination (%)			$\delta^{18}O$ (per mil V-SMOW)		
					Tephra	Clay	Total	$\delta^{18}O_{diatom}$	$\delta^{18}O_{modelled}$	±
4102	490	2.610263	2.609524	0.287	3.87	1.54	5.41	34.36	35.68	0.66
4103	500	2.610125	2.609389	0.468	6.76	18.34	25.09	26.09	30.41	2.16
4104	510	2.609988	2.609254	0.804	7.04	15.37	22.40	27.07	31.13	2.03
4105	520	2.609850	2.609119	0.343	3.04	18.29	21.33			
4106	530	2.609713	2.608984	0.302						
4108	540	2.609575	2.608849	0.239	7.22	17.23	24.46	27.63	32.34	2.36
4109	550	2.609438	2.608714	0.210	4.57	2.90	7.47	34.55	36.40	0.92
4110	560	2.609300	2.608579	0.619	4.73	23.22	27.95			
4111	570	2.609163	2.608444	0.326						
4112	580	2.609025	2.608310	0.158	5.49	21.54	27.03	29.06	34.83	2.88
4113	590	2.608888	2.608175	0.145						
4114	600	2.608750	2.608040	0.065	3.31	21.68	24.99			
4115	610	2.608613	2.607905	0.044	5.05	12.03	17.08	31.98	35.87	1.95
4116	620	2.608475	2.607770	0.067	1.71	31.23	32.94	28.62	35.73	3.55
4117	630	2.608338	2.607635	0.065	7.90	20.01	27.91	26.34	31.45	2.56
4118	640	2.608200	2.607500	0.076	3.48	16.67	20.15			
4119	650	2.608063	2.607400	0.100						
4121	660	2.607925	2.607300	0.041	2.48	18.31	20.78	30.35	34.68	2.16
4122	670	2.607788	2.607200	0.059						
4123	680	2.607650	2.607100	0.068	9.75	25.36	35.12			
4124	690	2.607513	2.607000	0.089						
4125	700	2.607375	2.606900	0.012	4.72	24.82	29.54	28.99	35.41	3.21
4126	710	2.607238	2.606800	0.308						
4127	720	2.607100	2.606700	0.026	6.48	24.03	30.51			
4128	730	2.606963	2.606600	0.055						
4129	740	2.606825	2.606500	0.017	10.79	28.77	39.56	26.72	35.59	4.43
4130	750	2.606688	2.606400	0.001						
4131	760	2.606550	2.606300	0.010	11.53	20.89	32.42			
4132	770	2.606413	2.606200	0.045						
4133	780	2.606275	2.606100	0.000	16.46	34.70	51.16	19.62	26.58	3.48
4134	790	2.606138	2.606000	0.030	22.97	29.64	52.61	16.18	20.31	2.06